Adatom controlled emergence of high hardness in biocompatible beta-Ti$_3$Au intermetallic thin film surfaces

Cecil Cherian Lukose [a], Ioannis Anestopoulos [b,c], Leon Bowen [d], Mihalis I. Panayiotidis [b,c], Martin Birkett [a,*]

[a] Department of Mechanical and Construction Engineering, Northumbria University, Newcastle Upon Tyne, UK
[b] Department of Cancer Genetics Therapeutics and Ultrastructural Pathology, The Cyprus Institute of Neurology and Genetics, Nicosia, Cyprus
[c] The Cyprus School of Molecular Medicine, The Cyprus Institute of Neurology and Genetics, Nicosia, Cyprus
[d] Department of Physics, G.J. Russell Microscopy Facility, Durham University, Durham, UK

ABSTRACT

There is growing international interest in hard biocompatible thin film surface coatings to extend the lifetime of medical implants. Parameters of the physical vapour deposition technique can be utilized to fine tune the microstructure and resulting properties of the growing thin film surface by modifying the adatom mobility of the incoming species. This work investigates the evolution of high hardness and biocompatibility of sputter deposited beta-Ti$_3$Au intermetallic thin film surfaces as a function of growth temperature and pressure. Titanium and gold are sputtered in an optimised 3:1 ratio over glass and Ti$_6$Al$_4$V substrates at varying pressures of 0.3 to 1.2 Pa and temperatures of 25 to 450°C. The microstructure and crystallinity of the deposited films improved with reduction in pressure from 1.2 to 0.3 Pa but development of the β-Ti$_3$Au intermetallic compound occurred at temperatures above 350°C. The density of the films also increased with reducing pressure, whereas improvement in their columnar structure was observed with increasing substrate temperature. These microstructural changes caused by adatom mobility variation, led to the emergence of superior mechanical surface hardness, reaching a peak value of 12.5 GPa for films grown at 0.3 Pa and 450°C. All thin film surfaces were highly biocompatible with ion leaching levels below 1 ppm, and films deposited at lower pressure exhibited much safer cytotoxic profiles against L929 mouse fibroblasts. This work demonstrates the emergence of high hardness and biocompatibility in Ti$_3$Au thin film surfaces with potential as next generation medical implant coating materials.

1. Introduction

Titanium (Ti) and its alloys like Ti$_6$Al$_4$V are used extensively in the manufacture of biomedical implants because of their excellent biocompatibility and corrosion resistance, especially for the fabrication of load bearing implants like total hip replacements (THR) and total knee replacements (TKR) [1–3]. However, the poor wear resistance of Ti$_6$Al$_4$V and the possibility of Al and V ion release can lead to premature loosening of the implant and other greater health problems [4–7]. Such failure of biomedical implant devices combined with prolonged life expectancy, are leading to a continuous increase in the number of reconstruction surgeries, which can be both high risk and painful for the patient and place a heavy financial burden on healthcare providers [1]. Therefore, there is an urgent need for super hard biocompatible coating materials to extend the service lifetime of Ti-based alloy implants [8,9].

The addition of noble metals has been shown to improve the mechanical properties of Ti-based alloys while maintaining the excellent biocompatibility of the individual elements [10,11]. The two most commonly alloyed elements for biomedical purposes are silver (Ag) [12, 13] and copper (Cu) [14–17] and they have been shown to increase the hardness of pure Ti by two fold [18–21]. They are also known for their excellent antimicrobial properties by inhibiting the formation of microbial biofilms [16,17,22] in the vicinity of the implant insertion. However, the prolonged presence of these materials within biological medium can lead to excessive leaching of their ions which are found to be extremely toxic to the host cells [23,24]. Gold (Au) is another highly biocompatible element belonging to the same family as Ag and Cu [25] and recent studies have found promising mechanical and biomedical performance in an bulk alloy system derived by alloying Au with Ti [26–29]. Compared to Ag or Cu, Au has a higher mass density, because

of its higher valence electron density, which results in an increased bond strength and in turn higher hardness, when alloyed with Ti [26]. Bulk TiAu materials prepared by arc melting were observed to give a sharp increment in mechanical hardness, reaching a peak value of 800 HV (~7.85 GPa) for samples with a stoichiometric ratio of Ti:Au of 3:1. This increase was assigned to the development of a super hard beta phase of the Ti_3Au intermetallic compound [26]. Karimi *et. al.* also found the hardness of TiAu thin films to peak when the Ti:Au atomic ratio is optimised to 3:1 and deposited at elevated substrate temperature, correlating very well with emergence of the Ti_3Au intermetallic [27]. Ti_3Au exists in two phases: α and β, and the calculated lattice parameter for the β-phase (~ 5.1 Å) is larger, with Ti existing in 14-fold coordination, which results in very high density of the formed unit cell for this phase of the Ti_3Au intermetallic. Compared to β, the α-phase has a smaller lattice parameter (~4.1 Å), and Ti exists in only 12-fold coordination [10,26] making the unit cell less dense. This difference between the coordination of Ti and Au atoms within the tightly packed unit cell presents a higher energy barrier for dislocation slipping within the lattice system, resulting in higher hardness for the β-phase of Ti_3Au compared to its α-phase counterpart [26]. These factors lead to enhanced hardness and low coefficient of friction for the β-Ti_3Au intermetallic, making it an ideal coating for orthopaedic implants [27]. Karimi *et al.* also proposed that preparing the β-Ti_3Au structure in thin film format will help to overcome the embrittlement issue arising because of the Pugh criterion (B/G < 1.75) as seen for bulk material samples [10,27,30]. The limited number of easy slip systems, larger Burgess vector, restricted cross slips and inability to transfer slips across grain boundaries, all make the Ti_3Au intermetallic more brittle and therefore more susceptible to cracking [10,27]. Von Mises yield criterion requires a minimum of five slip systems for a grain to be subject to deformation and become ductile, whereas Ti_3Au belongs to the A15 type lattice structure with reported slip activities along only three independent slip systems. Therefore, depositing thin film coatings of the Ti_3Au system on an underlying substrate like Ti_6Al_4V, will reinforce the integrity of the film. While the work of Karimi *et al.* presents mechanical aspects of Ti-Au thin films, there is still a requirement to investigate the biocompatibility of Ti-Au in thin film format and the resulting interrelationships between mechanical and biological performance.

In our previous work [31], we have clearly shown that superior mechanical hardness with excellent biocompatibility performance can be achieved for Ti-Au thin film coatings by optimising atomic ratios and thermal activation processes [27]. Thermal energy provided by in-situ substrate heating was found to be more efficient than ex-situ heat treatment in a tube furnace, to escalate the precipitation of the finely dispersed β-phase from the supersaturated α-phase, which act like

pinning sites resulting in precipitation hardening of the deposited Ti_3Au thin films [28]. However, there are many other deposition parameters like substrate temperature, gas pressure, target to substrate distance, substrate rotation speed, deposition angle, reactive gas pressure, target power level etc. which can all significantly affect the morphology, microstructure and performance of deposited thin films [32]. Prominent among these are deposition gas pressure and substrate temperature, which can be investigated using Thornton's structure zone model (SZM) which predicts the thin film texture with variation in these two key deposition parameters, as shown in Fig. 1 [33–35]. This model categorises deposited film textures and thus properties, to fall within one of four zones: (i) zone 1, (ii) zone T, (iii) zone 2 and (iv) zone 3, based upon the deposition pressure and homologous substrate temperature, which is represented by the ratio of T_{sub}/T_m, where T_m is the melting temperature of the deposited thin film and T_{sub} is the substrate temperature at which the film is deposited. With variation in deposition pressure, the texture of the deposited thin film is greatly affected which in turn leads to changes in thin film properties. For example, Ti thin films were observed to increase in surface roughness and electrical resistivity while the internal stresses shifted from tensile to compressive with increase in deposition pressure [36]. Similarly, increase in substrate temperature leads to enhancement of adatom mobility of the sputtered species reaching the substrate surface, thereby enabling them to orient preferentially. This results in organised growth which can be observed as changes in the columnar structure and crystallinity of thin films, clearly visible through characterisation techniques like SEM, TEM and XRD [34]. Therefore, by using this method, mechanical properties of materials can also be tuned by controlling the thin film texture. Previous studies have shown that TiN thin films deposited at elevated substrate temperature exhibit higher hardness [37,38] while Al-Si-N thin films have shown improved hardness when deposited at lower working gas pressures [39].

Here we propose a method to enhance the mechanical performance of biocompatible β-Ti_3Au thin films by improving the crystallinity and density through optimisation of key magnetron sputtering process parameters. We show how the combined effect of varying the substrate temperature and deposition pressure can lead to the development of super-hard and highly biocompatible Ti_3Au thin film coating materials suitable to extend the lifetime of next generation medical implant devices.
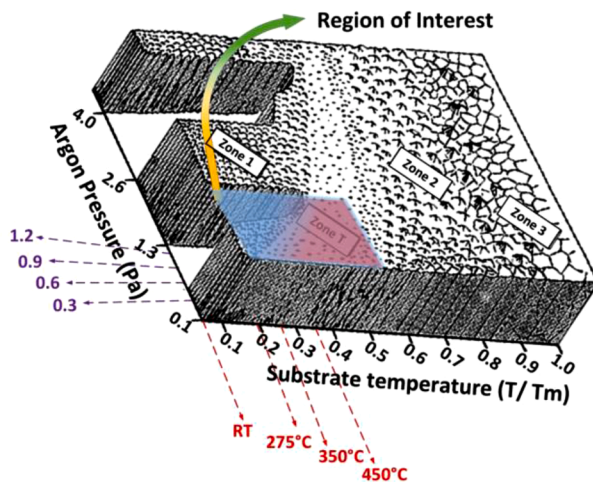
Deposition pressure (Pa)	Homologous Substrate temperature ($T_H = T_{sub}/T_m$, where $T_m = 1395°C$)	Predicted zone
< 0.5	$T_H < 0.1$	Zone 1
	$0.1 < T_H > 0.3$	Zone T
	$0.3 < T_H > 0.7$	Zone 2
	$T_H > 07$	Zone 3
0.5 <> 4	$T_H < 0.4$	Zone 1
	$0.4 < T_H > 0.5$	Zone T
	$0.5 < T_H > 0.7$	Zone 2
	$T_H > 07$	Zone 3

Fig. 1. Thorntons structural zone model (SZM) showing different zones and variation in thin film texture with variation in deposition pressure and homologous substrate temperature together with a table showing criteria to predict the zone of a thin film in Thornton's Structural zone model (SZM).

2. Materials and methods

2.1. Thin film deposition

Thin films of Ti$_3$Au alloy were sputtered onto glass and Ti alloy (Ti$_6$Al$_4$V) substrates using a NanoPVD deposition suite from Moorefield Nanotechnology. Rectangular Ti alloy substrates (76 mm by 26 mm and 1 mm thick) were polished using SiC paper from P240 to P4000 on a wheel polisher to a surface roughness of better than 40 nm, measured in either direction using an Alicona infinity focus surface measurement system. The polished Ti substates were then cut into three coupons measuring 25 mm by 19 mm (1 mm thick) using a guillotine. These Ti coupons were scrubbed, together with a set of glass slides (75 mm by 26 mm and 1 mm thick), using 1:5 Decon 90 agent, followed by ultrasonic bath cleaning with DI water. The cleaned substrates were then rinsed using IPA, acetone and a second ultrasonic bath before being blow dried using a jet of nitrogen. The cleaned substrates were loaded on a substrate holder within the sputtering chamber at a target to substrate distance of 100 mm. The chamber was loaded with 2-inch (50.8 mm) diameter circular targets made from 99.999% pure Ti and Au with the Ti target connected to a DC source, while the Au target was provided with an RF power source to slow down its deposition rate. The chamber was then evacuated to a base pressure better than 5×10^{-4} Pa and the substrate holder was rotated at a constant speed of 5 rpm.

To better understand the role of substrate temperature and deposition pressure, a full factorial design of experiment (DoE) was executed where these two parameters were varied over four individual levels, resulting in a total of 16 experimental conditions, as presented in Table 1.

Samples deposited without any substrate temperature were designated as RT (room temperature). Substrate heating was provided by a pair of halogen bulbs situated behind the substrate holder and a calibration was performed to correlate the halogen heater set point (SP) to the true temperature achieved on the substrate surface once it reached a steady state. It has been reported previously that crystallinity of Ti$_3$Au starts to improve with substrate temperatures above 270℃ [27], therefore the DoE was set to explore temperature ranges above this particular point. After the RT samples, the lower limit for substrate heating was set at 275℃ (400SP), followed by an intermediate point of 350℃ (500SP) and thereafter, the upper limit of 450℃ (600SP) was defined by the heaters maximum set point. The deposition pressure of the system was controlled by the Ar flow within the chamber during deposition and in our previous work a set pressure of 0.6 Pa (Ar flow of 10 sccm) was used [31]. Therefore, for this work we explored the effect of varying deposition pressure from 1.2 Pa (Ar flow of 20 sccm) down to 0.3 Pa, (Ar flow of 5 sccm). The upper level of 1.2 Pa was set by the 4-level nature of the experimental design, while the lower level of 0.3 Pa was the minimum pressure at which a plasma could be maintained.

2.2. Thin film characterisation

The microstructure of the deposited thin films was characterised by the X-ray diffraction (XRD) technique using a Rigaku Smart Lab 2 X-ray diffractometer, equipped with Cu K$_\alpha$ radiation, in parallel beam configuration. The reflection patterns were collected between 2θ values of 10 and 80° and the peaks were indexed using the inbuild crystallographic data base and verified with files from the ICSD (Inorganic Crystal Structure Database). The morphology of the sample surfaces and cross section regions were analysed using high resolution images generated by a MIRA 3 scanning electron microscope (SEM) from Tescan systems, operating at 5 kV and a working distance of 5 mm from the e-beam lens. Elemental composition of each sample was verified using an Oxford instruments X-Max 150 energy dispersive X-ray (EDX) spectroscopy detector built within the SEM. Transmission electron microscope (TEM) lamellar were prepared by focused ion beam (FIB) milling using a FEI Helios Nano Lab 600 Dual Beam system, equipped with a focused 30 keV Ga liquid metal ion source. TEM imaging was obtained with a JEOL 2100F TEM operated at 200 KeV. Micro-analysis was obtained at 200 KeV, 0.7 nA in scanning transmission operation using an Oxford Instruments micros-analysis system. Hardness and elastic modulus were measured by performing nanoindentation using a 3-sided Berkovich tip made of diamond, employed within a Bruker-Hysitron TI900-Triboindneter nanomechanical testing system. For each sample, a set of 16 indentations in a 4×4 pattern was made, with 10 μm spacing between each indent. Each indent was controlled to achieve a depth around 10% of the total film thickness to avoid any effect form the underlying substrate. Following the Oliver and Pharr indentation method, the force-displacement curve was plotted for each indent and the unloading curve was analysed to extract the required mechanical data. The surface roughness and grain size of the films were estimated using a Nanoveeco Dimension 3000 atomic force microscope (AFM) by scanning a 15 nm sharp silicon tip in continuous contact mode over a surface area of 3×3 μm.

2.3. Cell lines and culture reagents

L929 murine fibroblast cells were purchased from Deutsche Sammlung von Microorganismen und Zellkulturen (DSMZ – Braunschweig, Germany). Cells were cultured in Dulbeccos's Modified Eagle Medium (DMEM), high glucose, supplemented with 10% fetal bovine serum (FBS), 2 mM L-glutamine, 100 U/ml penicillin and 100 μg/ml streptomycin, while incubated under humidified conditions at 37°C and 5% CO$_2$. L929 cells were grown as monolayer cultures, while when confluency reached 80–90%, cells were sub-cultured for a maximum of 20-25 passages, before new vials were used. All cell culture media and reagents [foetal bovine serum (FBS), antibiotics, trypsin, Phosphate Buffer Saline (PBS)] were obtained from Biosera (Kansas City, MO, USA), while for cytotoxicity assays, Resazurin sodium salt was purchased from Fluorochem (Derbyshire, UK).

2.4. Thin film extracts preparation

In order to obtain different thin film extracts, two distinct experimental protocols were followed. Specifically, a first set of extracts was prepared through immersion of thin film test samples into 6-well culture plates containing 6 ml of DMEM media for 72 hours in a humidified incubator at 37°C, 5% CO$_2$. In addition, a slight agitation was applied to the 6-well plates containing the samples for 5 seconds at the beginning

Table 1
Parameter levels for substrate temperature and deposition pressure with the resulting film thickness and elemental composition achieved.

Sample ID	Substrate temperature (C)	Deposition pressure (Pa)	Film thickness (nm)	Elemental composition (at%)	
				Ti	Au
S$_{RT-3}$	RT	0.3	692	75.5	24.5
S$_{RT-6}$		0.6	533	74.9	25.1
S$_{RT-9}$		0.9	536	73.9	26.1
S$_{RT-12}$		1.2	495	75.7	24.3
S$_{275-3}$	275	0.3	681	75.4	24.6
S$_{275-6}$		0.6	676	73.8	26.2
S$_{275-9}$		0.9	486	73.9	26.1
S$_{275-12}$		1.2	485	74.6	25.4
S$_{350-3}$	350	0.3	690	76.4	23.6
S$_{350-6}$		0.6	571	73.9	26.1
S$_{350-9}$		0.9	495	74.8	25.2
S$_{350-12}$		1.2	527	76.3	23.7
S$_{450-3}$	450	0.3	623	73.9	26.1
S$_{450-6}$		0.6	593	75.3	24.7
S$_{450-9}$		0.9	641	74.7	25.3
S$_{450-12}$		1.2	482	76.4	23.6
Mean			575.3	74.9	25.1
Std Deviation			78.4	0.9	0.8

and the end of the preparation period, in order to achieve sufficient ion leaching rates in culture media, that were subsequently used for cytotoxicity experiments against L929 mouse fibroblast cells. Accordingly, a second set of extracts from the same thin films was obtained following an additional incubation period of 96 hours into DMEM media, following the completion of the initial 72 hours leaching time. In addition to the thin film extracts, extracts derived from polished Cu and Ti substrates were used as positive and negative control samples, respectively, for the cytotoxicity experiments.

2.5. Biocompatibility characterisation of thin films against L929 mouse fibroblast cells

The biocompatibility properties of the deposited thin films were analysed by measuring their in-*vitro* cytotoxic effect and ion leaching potential according to ISO 10993 standards. The process cycle for cell viability assessment using the Alamar blue assay is shown in Fig. 2. Specifically, L929 cells were plated at a density of 2000 cells/well into a 96-well culture plate and incubated overnight. The following day DMEM culture media was replaced with extracts obtained from thin films deposited on titanium substrates, following 72 and 168 hour ion leaching periods. In each experimental condition, L929 cells were exposed to both types of leached extracts for a total period of 72 hours. In parallel, exposures of L929 cells to both Cu substrate derived and 10% DMSO containing extracts were used as positive control conditions, while negative control samples consisted of L929 cells exposed to pure DMEM media (Blank samples) as well as extract leached from a blank Ti substrate. Next, following completion of 72 hour incubations, 10 µl of resazurin (1 mg/ml final concentration) was added in each well and the cells were incubated for 4 hours at 37°C. Finally, absorbance measurements were performed at 570 and 590 nm (reference wavelength) using an absorbance plate reader (Labtech LT4500, UK). Cell viability levels were calculated and expressed as a percentage of untreated (BLANK) cells.

Ions leached from Ti₃Au thin films and blank Ti and Cu substrates into the extracts were measured using a Perkin Elemer Optima 8000 inductively coupled plasma optical emission mass spectrometer (ICP-OEMS). A portion of the extracts prepared from these samples were passed through the mass spectrometer and the results were compared against a set of calibrated standards containing 0.625, 2.5, 5.0 and 10 ppm of dissolved Ti, Al, V, Cu and Au.

3. Results

3.1. Structural and chemical characterisation

The elemental compositions of the Ti₃Au thin films deposited at varying substrate temperature and deposition pressure, measured using EDX analysis are presented in Table 1, together with the film thickness measured from the cross-section SEM images presented later in Fig. 4b. The thickness of the films appears to be less affected by variation in substrate temperature but varies strongly with change in deposition pressure. For any substrate temperature, films deposited at 0.3 Pa register film thickness above 650 nm, which decrease to mid-500 nm thicknesses for 0.6 Pa and then reduces to the lower 500 nm or upper 400 nm range with further increase in deposition pressure to 0.9 and 1.2 Pa. It is well documented that the mean free path reduces at higher gas pressure leading to increased probability of collisions between the target species ejected and the Ar ions in the plasma. This leads to a reduction in energy of the sputtered species causing its deflection from the deposition area, resulting in reduced film thickness at higher gas pressures [40–42].

On the other hand, the elemental composition is seen to be much more consistent throughout the design of experiment, irrespective of deposition pressure or substrate temperature. Between deposition runs, it was observed that change in deposition pressure shifted the atomic composition of the TiAu films further from the required 3:1 ratio. Therefore, those runs had to be repeated with slight adjustments in the power levels of the individual targets to achieve the required composition. Therefore, in the final set of 16 samples, an average Ti to Au ratio of 74.9:25.1 at% is achieved, with a standard deviation of 0.90 at% between all 16 deposited samples. For any one individual sample the maximum variation in elemental composition never deviates more than 1.4 at% from the required 75 at% Ti or 25 at% Au. From our previous work [31], it was observed that the microstructure remains very similar for variation in Au concentration up to 3 at% in the film, therefore the small deviation of less than 1.5 at% observed in these samples is ideal for comparison of structural, morphological, mechanical and biomedical properties.
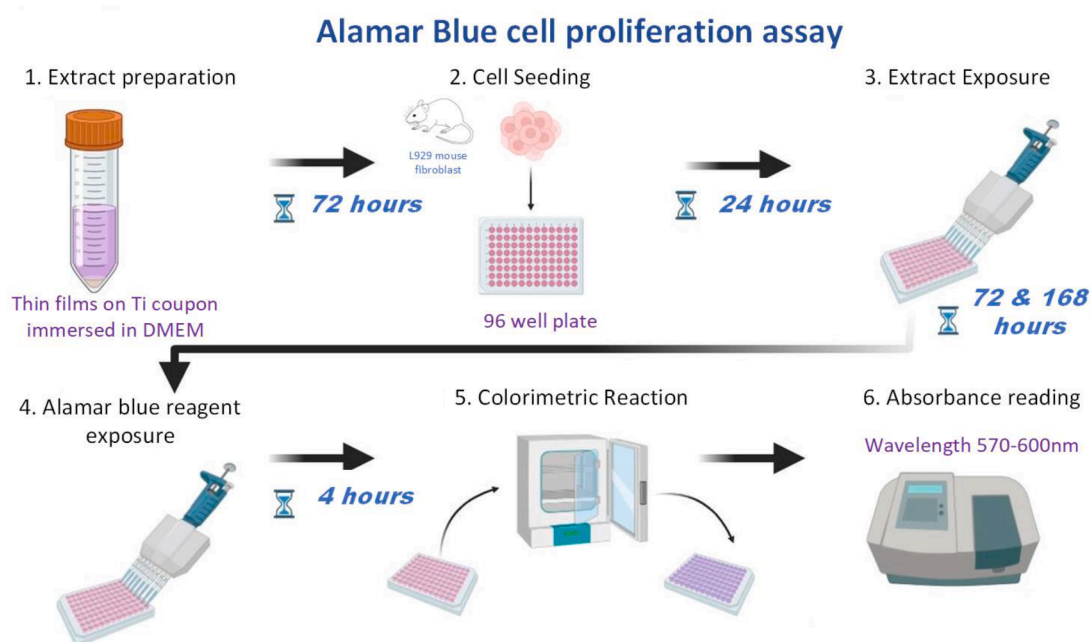

Fig. 2. Process cycle for measuring cell viability of L929 mouse fibroblast cells on exposure to extracts prepared from Ti₃Au thin films using Alamar blue reagent.

The effect of deposition pressure on the structural development of Ti_3Au thin films deposited on glass, for varying substrate temperatures is shown in Fig. 3 (a-d). The purple reference line shows the expected peak location (and all Miller indices in Fig 3a for reference) for the β-phase of the Ti_3Au intermetallic compound according to the ICSD database (collection no: 58605). Samples deposited at room temperature (S_{RT-6}, S_{RT-9} and S_{RT-12}) show very broad peaks which are indicative of their nano-crystalline nature and are expected for thin films deposited without substrate temperature due to reduced adatom mobility, in addition to high deposition pressure which further reduces the energy of incoming species due to collisions along their flight path [34]. However, with decreasing deposition pressure from 1.2 to 0.6 Pa, a broad peak can be observed to develop around 40° which becomes extremely well defined with further reduction of deposition pressure to 0.3 Pa. The broad peak appearing at lower adatom mobility has been observed before [27,31] and is assigned to the coexistence of various Ti-Au intermetallics, all of which have one characteristic peak in the 2θ region between 36 to 42° [27]. However, the peak seen in the S_{RT-3} sample is located at 37.6°, which is a very close match to the (111) plane of the

α-phase of the Ti_3Au intermetallic, suggesting development of the Ti_3Au intermetallic with decreasing deposition pressure. This improved crystalline quality at lower gas pressure results from the reduced number of collisions between ejected species and gas particles in the plasma which in turn increases the energy of the ejected species from the target [43, 44]. These higher energy ejected species in turn have higher probability of migrating to nucleation sites when they reach the substrate surface, resulting in better crystallization of thin films at lower gas pressure [45, 46]. Considerable improvement in crystallinity can also be seen with increment in substrate temperature. Even the sample deposited at higher deposition pressure (S_{275-12}) has a clear peak positioned at 37.5°, though this peak belongs to α-Ti_3Au. However, increment in adatom energy brought by further reduction of deposition pressure for samples deposited at 275°C substrate temperature (S_{275-9} and S_{275-6}), is sufficient to initiate development of the β-phase of the Ti_3Au intermetallic, confirmed by the presence of diffraction peaks located at 35.3°, 39.6° and 74.6°, representing the (200), (210) and (400) planes respectively. The peak positioned at 37.4° suggests that some amount of α-phase is also intermixed with the β-phase. While the intensity of this peak steadily

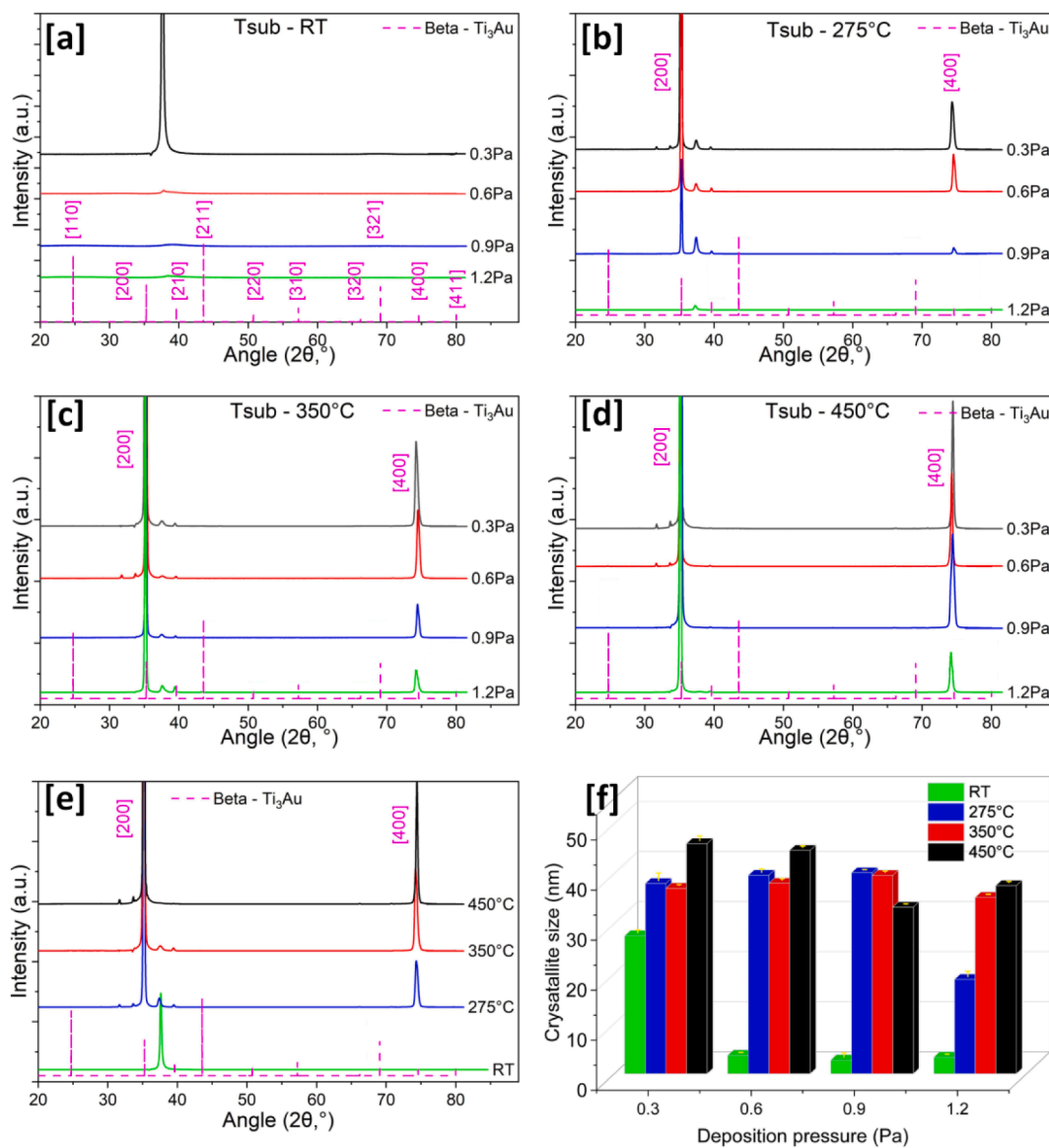**Fig. 3.** Diffraction patterns for Ti_3Au thin films deposited on glass substrates at varying deposition pressure and constant substrate temperatures of (a) RT (b) 275°C (c)350°C (d) 450°C, and (e) at varying substrate temperature and a constant deposition pressure of 0.3 Pa. (e) graph showing calculated crystallite size of Ti_3Au thin films deposited with varying deposition pressure and substrate temperature.

decreases with reduction in deposition pressure, the intensity of the (400) plane of the β-phase (74.6) increases with the same reduction in pressure and suggests that with sufficient energy, the ejected species favour the precipitation of the β-phase over the α-phase. For samples deposited at 350℃ substrate temperature, formation of the β-phase takes place regardless of the deposition pressure, with peaks of the β-phase intensifying with reduction in deposition pressure. Though the α-phase is still present at higher deposition pressure (S$_{350-12}$), it consistently decreases in intensity with reduction in deposition pressure, for the reasons explained before. With the reduction in deposition pressure, the peak located at 39.6° representing the (210) plane of the β-phase also reduces, indicating a shift from polycrystalline nature to preferential orientation along the [100] family of planes. For thin film samples deposited at a substrate temperature of 450°, high intensity, single phase β-Ti$_3$Au with preferential orientation along the [100] family of planes is observed, independent of deposition pressure.

Fig. 3 (e) compares the diffraction patterns of films grown at the lowest deposition pressure of 0.3 Pa, at varying substrate temperatures to clearly outline the stages of Ti$_3$Au intermetallic development with variation in deposition parameters. Increasing the deposition temperature increases the mobility of the adatoms while also reducing the surface diffusion length, which ultimately builds up the adatom energy [27]. Adatoms with enhanced energy can migrate more easily towards lattice sites on the substrate surface, leading to the development of thin films with better crystallinity, as seen with the development of preferentially oriented β-Ti$_3$Au at 450℃ compared to strained α-Ti$_3$Au achieved at room temperature deposition. Fig. 3(f) shows a comparison of crystallite size calculated using Scherrer`s equation, from the highest intensity peaks in the diffraction patterns for the 16 samples [47]. The nano-crystalline nature of the thin films deposited at room temperature is clearly evident with crystallite sizes less than 3 nm, though the film deposited at 0.3 Pa registers crystallite sizes around 27 nm due to the formation of the α-phase. Increasing substrate temperature favours formation of larger 18 nm crystals even at the highest deposition pressure of 1.2 Pa. For the rest of the films deposited at 275 and 350℃, the crystallite size shows moderate variation in the range of 33 to 40 nm. Samples deposited at a substrate temperature of 450℃ and at deposition pressure lower than 0.6 Pa show the largest crystallite sizes of around 45 nm. Therefore, results thus far clearly show that formation, quality and ratio of α and β phases of Ti$_3$Au in the thin film and their crystallite size, can be controlled by tuning deposition process parameters like gas pressure and substrate temperature.

### 3.2. Surface and cross section characterisations

SEM surface images of Ti$_3$Au thin films deposited on glass at varying substrate temperature and deposition pressure are presented in Fig. 4 (a). For samples deposited at room temperature, the thin film surface exhibits extremely fine powdered texture, which is expected from the quasi-crystalline nature of the thin metallic films. Within this row, some random surface features are visible when the deposition pressure is reduced to 0.3 Pa, corresponding with the emergence of a sharp peak in the diffraction pattern seen earlier. With increment in substrate temperature to 275℃, the film deposited at 1.2 Pa depicts circular dome shaped features with larger separation between grain boundaries. With reduction in deposition pressure to 0.9 Pa, two different zones are visible: a smooth glass like zone and clusters of small circular grains. The emergence of this clearly distinctive zone corresponds with the XRD pattern which shows coexistence of α and β phases of the Ti$_3$Au intermetallic at these deposition parameters. With further reduction in pressure to 0.6 and 0.3 Pa, coverage of circular grains increases drastically and represents the continuous growth of the β-phase with reduction in pressure. When the substrate temperature is increased to 350℃, smooth versus grainy distinction is clearly visibly even at the highest deposition pressure of 1.2 Pa and again the coverage of the circular grainy phase increases with reducing deposition pressure. For the films

deposited at the highest substrate temperature of 450℃, circular grains give way to form angular edges and sharp facets, signifying development of well oriented good quality β-Ti$_3$Au crystals, as also shown by the XRD pattern for this sample. But with further reduction in deposition pressure, grains revert to dome shaped with extreme densification of the film.

Thornton`s SZM predicts the texture and microstructure of thin films by classifying them into four zones, according to their deposition pressure and the homologous substrate temperature (T$_{sub}$/T$_m$), which is the ratio of the substrate temperature (T$_{sub}$) to the melting temperature (T$_m$) of the alloy under test [34]. From the Ti-Au phase diagram the melting point of Ti$_3$Au alloy is known to be 1395℃ [27,48], and can be used together with the substrate temperatures of RT (25℃ ambient), 275, 350, and 450℃ used in this experiment to calculate their homologous substrate temperature values of: 0.01, 0.19, 0.25 and 0.32 respectively. By comparing the SZM prediction criteria given in Fig. 1, we can see that samples deposited at the lowest deposition pressure of 0.3 Pa can transition between different zones with a smaller increase in the homologous temperature compared to those grown at deposition pressures higher than 0.5 Pa [34]. Therefore, it can be said that S$_{450-3}$ belongs to zone 2, S$_{350-3}$ and S$_{275-3}$ belong to zone T and the rest of the thin film samples belong to zone 1 of the SZM. Thin films deposited at low substrate temperature and high deposition pressure fall into zone 1 and depict open voided structures with an amorphous nature. At high deposition pressures, the collision rate between sputtered particles and gas particles is high, which results in low angle oblique incidence of sputtered target species. When combined with low substrate temperature, which leads to low mobility of adatoms on the substrate surface, the resulting structure is amorphous in nature.

The change in the texture of the film becomes even clearer when its cross section is analysed using SEM, as shown in Fig. 4(b). The open voided and broken pillar like structure is evident for films deposited at the highest deposition pressure of 1.2 Pa without substrate temperature (S$_{RT-12}$). For films deposited at room temperature, a reduction in deposition pressure brings significant change to the film texture, transitioning from a columnar pillar like structure at 0.6 Pa to extremely dense glass like at 0.3 Pa. With increase in substrate temperature, a better columnar structure starts developing even for the films deposited at 1.2 Pa and further improvements in column formation can be seen with reduction in pressure to 0.9 Pa. Thin films deposited at 0.6 Pa are on the border of transitioning to zone T of the SZM and therefore depict some characteristic traits of this zone, like well-formed and denser columns with flat surfaces. These surface features are a result of increase in substrate temperature which enhances thermally driven diffusion on the substrate surface, together with reduction in deposition pressure which leads to higher energy of the incoming sputtered species. Better surface diffusion leads to denser packing of columns with a smoother film surface. Samples deposited at the lowest deposition pressure of 0.3 Pa and homologous substrate temperature of 0.32 (S$_{450-3}$), transition into zone 2, marked by denser and wider columns. Because of the increase in substrate temperature, surface and grain boundary adatom diffusion leads to broadening of the columns and subsequent reduction of voids between them. The higher energy of incoming species promotes significant crystallographic development of columns in the preferred orientation, which is in total agreement with the XRD results seen earlier for this sample.

Too gain a deeper understanding of the effects of deposition pressure and substrate temperature on the underlying columnar structure, thin film samples deposited from the four extreme corners of the DoE matrix (S$_{RT-3}$, S$_{RT-12}$, S$_{450-3}$ and S$_{450-12}$), were FIB milled and imaged under a TEM. Brightfield images of these samples are presented in Fig. 5 (a) while their darkfield counterparts are available in supplementary data 3. Fig. 5 (a) shows that even at room temperature, samples deposited at lower pressure (S$_{RT-3}$) show the presence of tall columnar structures extending through the film thickness, supporting the crystalline nature of films at lower deposition pressure seen in the XRD patterns earlier. On
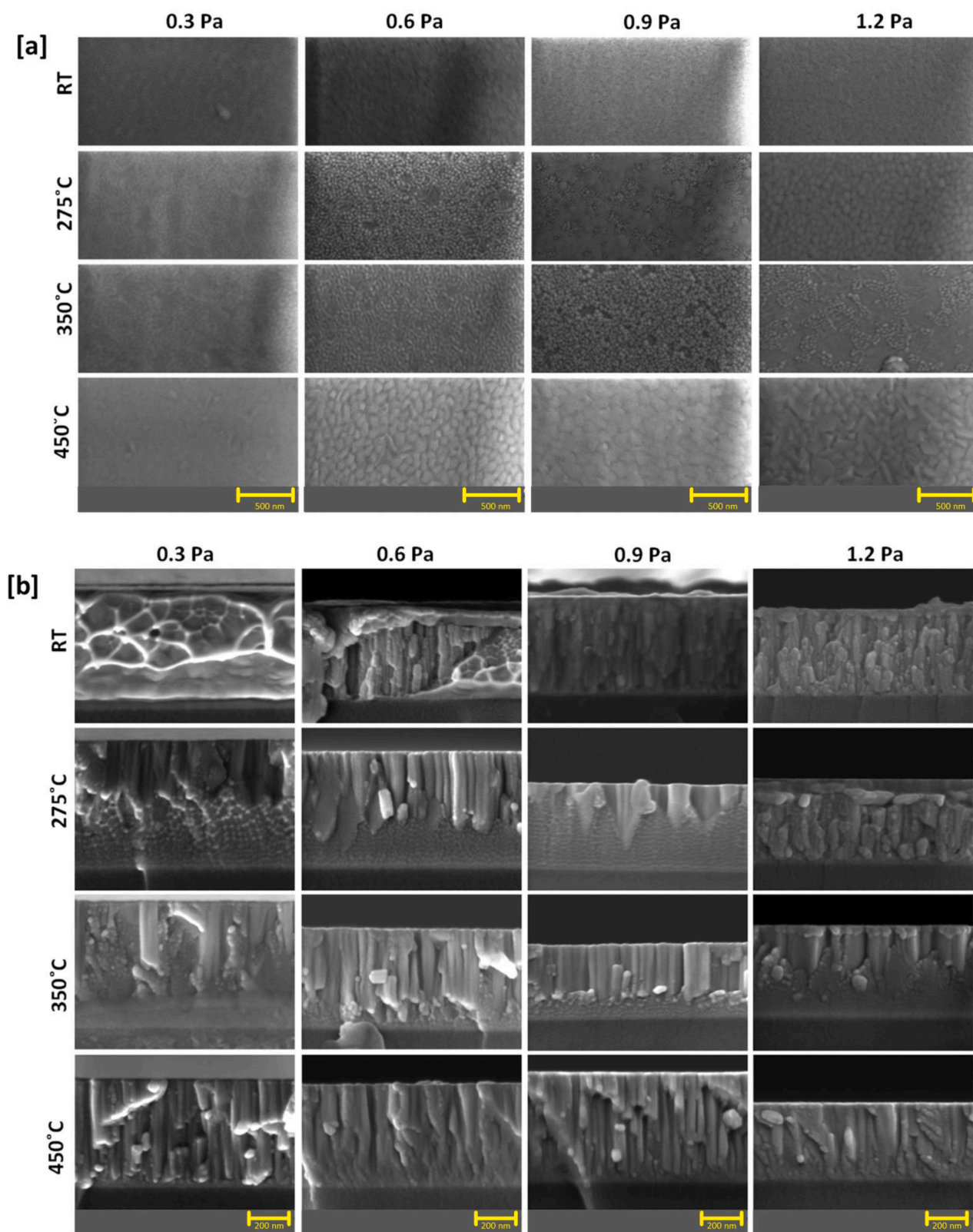
Fig. 4. (a) Surface images of Ti₃Au thin films deposited on glass substrates with increasing deposition pressure (moving horizontally, left to right) and with increasing substrate temperature (moving vertically, top to bottom). (b) Cross section images of Ti₃Au thin films deposited on glass substrates with increasing deposition pressure (moving horizontally, left to right) and with increasing substrate temperature (moving vertically, top to bottom).
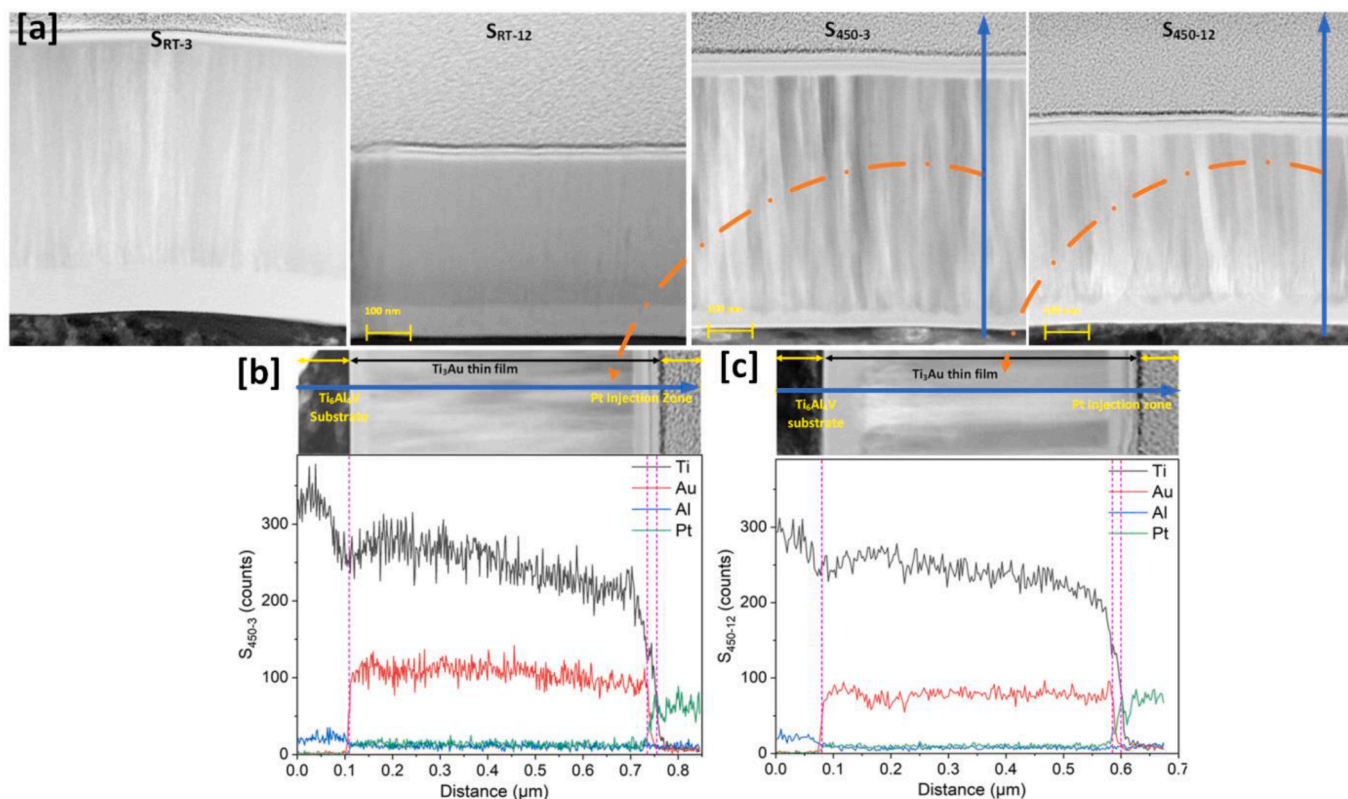
Fig. 5. (a) Brightfield TEM images of samples S_{RT-3}, S_{RT-12}, S_{450-3} and S_{450-12} showing development of columnar microstructure with decreasing deposition pressure and increasing substrate temperature. Elemental depth profiles of (b) S450-3 and (c) S450-12) developed from EDX analysis of TEM cross sections.

the other hand, the amorphous nature of sample S_{RT-12}, also seen earlier in diffraction patterns, is yet again supported by the absence of any visible grain features under TEM analysis. However, with increase of substrate temperature, even the film deposited at higher deposition pressure.

(S_{450-12}) shows clear development of columnar features. One interesting observation for all four samples is the merging of the columnar features into a continuous band at the film-substrate interface. This parallel band decreases in size with increasing temperature and crystallization and appears to be weakest for sample S_{450-3}, where the film crystallization is observed to be strongest with well-defined and densely packed columns.

In order to understand the elemental nature of the band observed at the film-substrate interface, an EDX depth profile was performed as a line scan through the thin film cross-sections during the TEM imaging of samples S_{450-3} and S_{450-12} (represented by blue arrows in Fig 5a) and the results for each element are presented in Fig. 5 (b) and (c), respectively. Both images are very similar in nature showing three distinctive zones, moving from left to right through: Ti_6Al_4V substrate, Ti_3Au thin film and Pt injection. The substrate region is characterised by elevated Ti and Al levels as expected from a Ti_6Al_4V substrate, while vanadium presence was below detection limits. Al undergoes a sharp decline approaching the film-substrate interface, at which point Ti and Au increase to their peak levels. Au maintains a consistent value throughout the film thickness, while Ti counts are observed to be slightly higher near the film-substrate interface and gradually reduce towards the film surface. This reduction is indicative of diffusion of Ti taking place across the film interface and could be corelated to the continuous band observed in this region in the TEM images (Fig 5a). Au and Ti counts both drop at the film surface and are replaced by the Pt injection, which is an artefact of the FIB/TEM procedure. The total film thickness measured from the line scans of S_{450-3} and S_{450-12} are around 640 and 510 nm respectively and match very closely to the values measured from the SEM cross section

method, reported in Table 1.

As explained above, varying deposition pressure and substrate temperature leads to variation in surface roughness of the deposited Ti_3Au thin films and this variation was measured using an AFM by rastering a sharp silicon tip over a 3×3 μm surface area. The AFM scan images for the thin films, shown in Fig. 6 (a), give an estimate of the largest surface feature size, while variation of colour gives an estimate of the uniformity of film surface roughness. For samples deposited at the lowest pressure of 0.3 Pa, the sputtering species encounter fewer Ar ions during their flight path which reduces interspecies collisions in the transition path from the target to substrate, leading to higher energy of the bombarding species, making the resulting surface flatter. The flatness of the surface improves with increasing substrate temperature, which is explained by the increased energy for surface and grain boundary diffusion. On the other hand, films deposited at higher pressure, in the absence of sufficient substrate temperature, tend to form typical zone 1 amorphous or quasi crystalline structures with smoother glass like surfaces. Contrary to these two extremes, samples deposited at an intermediate deposition pressure and substrate temperature (within blue rectangle in Fig 6a) show higher surface roughness. This is because films deposited at intermediate pressure ranges have improved crystallinity when compared to films grown at higher deposition pressure which are known to be amorphous. However, because of the relatively high number of Ar ions, interspecies collisions are still not reduced enough to promote flatter film surfaces, resulting in more pronounced surface roughness for the films deposited at intermediate pressure ranges. The film deposited at the highest substrate temperature (450℃) and lowest deposition pressure (0.3 Pa) exhibits the best uniformity of surface features as indicated by the uniform colour and the lowest grain feature heights for that sample.

Fig. 6(b) gives the quantified value of mean surface roughness values measured from the AFM scans in Fig. 6(a). It can be clearly seen that samples deposited at room temperature and 450℃ report the lowest surface roughness values, which reduce further with decrease in
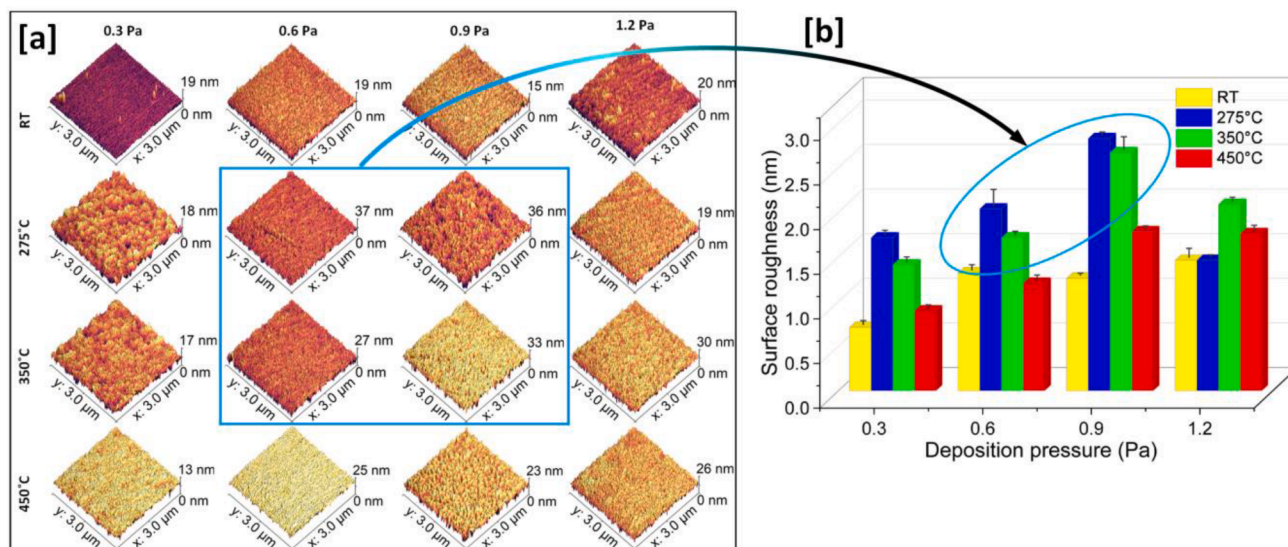
Fig. 6. (a) AFM surface profiles of Ti$_3$Au thin films deposited on glass substrates with increasing deposition pressure (moving horizontally left to right) and with increasing substrate temperature (moving vertically from top to bottom). Blue rectangle highlights Ti$_3$Au thin films deposited at intermediate pressure and substrate temperature. (b) Bar chart showing mean surface roughness measured from AFM scans in Fig 6a using Gwydion software.

deposition pressure. Whereas the films deposited at intermediate substrate temperatures exhibit higher surface roughness, which is again observed to reduce with decreasing deposition pressure. The combination of surface roughness and grain height gives an estimated variation in the grain size with deposition parameters. So, from the XRD, SEM and AFM results, it can be concluded that the β-Ti$_3$Au film with the most preferential orientation, densest columnar structure, smaller grain features and smoother surface roughness is formed when deposited at the highest substrate temperature of 450°C and the lowest deposition pressure of 0.3 Pa.
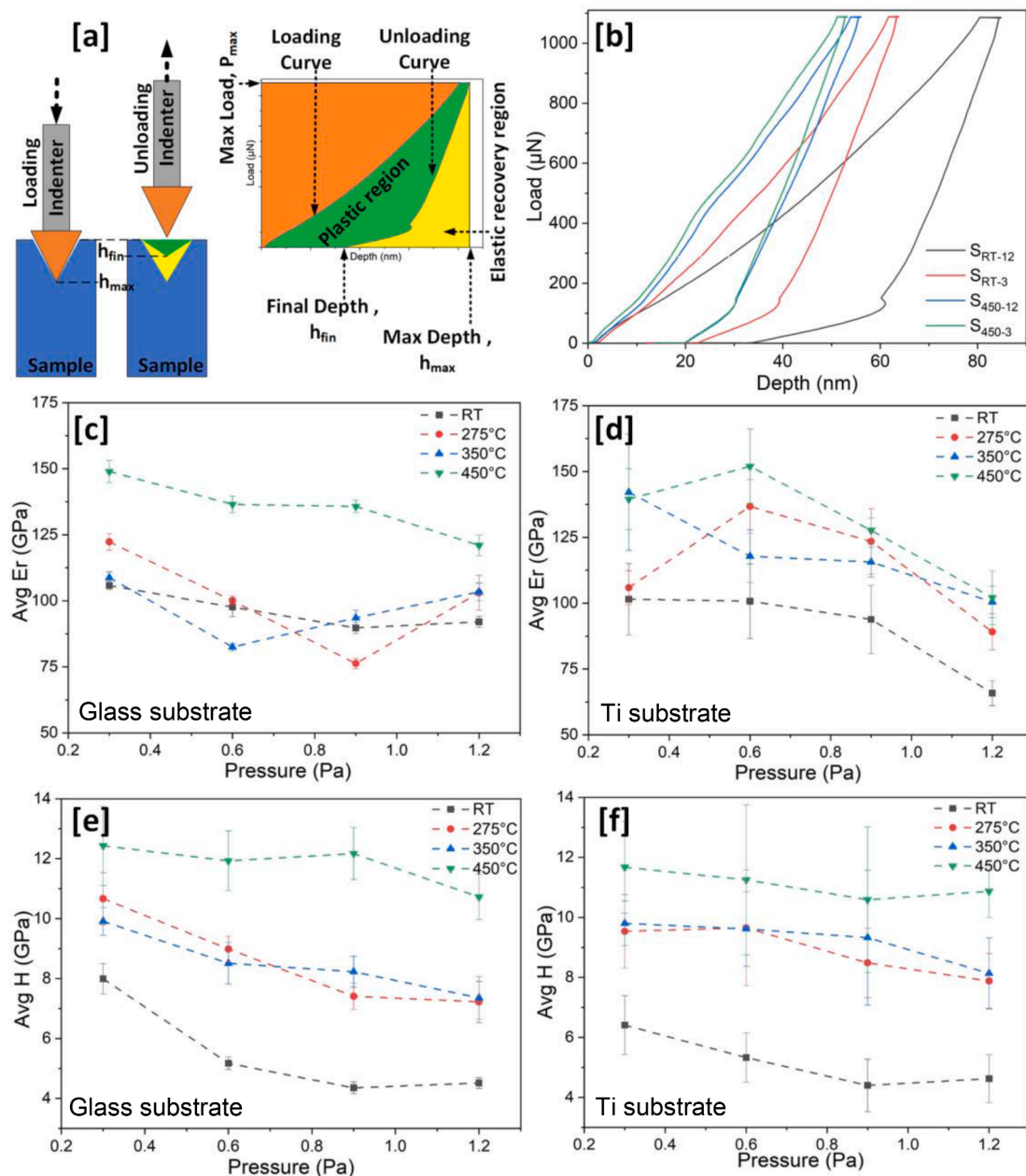
3.3. Mechanical characterisation

Fig. 7(a) shows a schematic representation of the nanoindentation process corelated to various regions of the generated load-displacement curve, while Fig. 7(b) displays the load displacement curves of four of the Ti$_3$Au thin film samples: S_{RT-3}, S_{RT-12}, S_{450-3} and S_{450-12}, showing the effect that the deposition parameters have on the interaction taking place between the indenter tip and the thin film surface. For the sake of comparison, all of these curves are taken from samples deposited on glass substrates and these indentations are all made at a constant load of 1100 μN with a load dwell and unload time duration of 10 seconds each. These curves do not show any sudden shift of displacement along the x-axis, commonly known as "staircase phenomenon" or displacement excursions [49,50]. These phenomena are recorded if the indenter tip interacts with surface contamination, or different phases or oxide layers which differ in mechanical properties from the main underlying film [51]. Samples deposited with in-situ substrate temperature are not prone to oxidation and thorough cleaning of the samples ensures that no surface contaminants are present. While different phases of the Ti$_3$Au intermetallic exist, if these discontinuities do not separate from each other when under load, they can still support the continuous progression of the indenter tip into the film, which will result in smooth and event free load displacement curves, as seen in Fig. 7(a) [52].

At the peak of the load, the indenter tip travels a maximum indentation depth in excess of 80 nm through sample S_{RT-12} (black curve in Fig 7b) and analysing the unloading curve shows that the resulting contact depth is 68 nm, with a reduced elastic modulus (Er) of 91.5 GPa and mechanical hardness (H) of 4.76 GPa. However, sample S_{RT-3} (red curve), deposited at the lowest deposition pressure of 0.3 Pa, shows a marked improvement in film hardness, offering more resistance to tip

penetration for the same load, with maximum displacement just above 60 nm. This translates to a contact depth of 46 nm with values of Er and H of 115 GPa and 7.96 GPa respectively. Samples S_{450-12} and S_{450-3} (blue and green curves), deposited at higher substrate temperature, present load displacement hysteresis, getting thinner with reduction in deposition pressure, clearly showing the improvement in mechanical performance with increasing substrate temperature and decreasing deposition pressure. Contact depths extracted from their unloading curves decrease from 36.9 to 35.8 nm, while mechanical hardness increases from 10.8 to 11.9 GPa with reduction in deposition pressure from 1.2 to 0.3 Pa. The area under the P-H curve represents the work done by the indenter tip to create a plastic deformation within the thin film surface and the hysteresis in this curve is caused by the elastic recovery of the unloading curve, which depends heavily upon the nature of the thin film [53,54]. Depositing thin films at lower deposition pressure and higher substrate temperature leads to higher adatom mobility and better grain boundary diffusion resulting in denser and better crystallised thin films, as evident from the SEM and XRD results earlier. Films with better crystallization undergo less elastic recovery or reduced mechanical hysteresis caused by plastic deformation, i.e. they become stiffer and harder [54]. While the P-H curves are helpful to understand and compare the mechanical performance of individual indents, to narrow down optimised substrate temperature and deposition pressure to achieve Ti$_3$Au thin film coatings with peak mechanical performance, the average values of elastic modulus and hardness are analysed next.

Reduced elastic modulus from nanoindentation of the Ti$_3$Au thin film samples deposited on glass substrates with varying deposition pressure and substrate temperature are shown in Fig. 7 (c). Reduced elastic modulus accounts for elastic deformation taking place on the test material and the indenter tip material without the need for Poison`s ratio, thus easing the analysis of the results [11]. Ti$_3$Au thin films despotised at room temperature, report an increasing trend for reduced elastic modulus from 92±2 to 105±1.5 GPa, when the deposition pressure is reduced from 1.2 to 0.3 Pa. Increasing the substrate temperature to 275 and 350C, leads to a reduction in elastic modulus in the intermediate deposition pressure range of 0.9 to 0.6 Pa, before it increases again for the lowest pressure of 0.3 Pa, reaching 122±3 and 108±2 GPa respectively. One factor responsible for this dip in elastic modulus at intermediate pressures could be the surface roughness of these particular films deposited at 275 and 350C. In previous sections it has been explained that thin films deposited at intermediate substrate

Fig. 7. (a) Schematic of the nanoindentation process corelated to various regions of the generated load-displacement curve. (b) Load-displacement curves for Ti₃Au thin film samples at four extremes of the DoE, showing effect of deposition parameters on the interaction of the indenter tip with the film surface. (c-f) Plots of variation in reduced elastic modulus (Er) and mechanical hardness (H) of Ti₃Au thin films deposited on glass and Ti substrates with varying substrate temperature and deposition pressure.

temperature and deposition pressure depicted a rise in surface roughness and many earlier studies have observed a reduction in elastic modulus with increment of surface roughness due to the indenter size effect [55,56]. Samples deposited at the highest substrate temperature of 450℃, report elastic modulus values higher than 120±4 GPa and continuously increase with reducing deposition pressure reaching a peak value of 149±4 GPa for films deposited at 0.3 Pa.

Curves for mechanical hardness of the Ti₃Au thin film samples deposited on glass substrates (Fig 7e) present better distinction between the samples deposited at varying substrate temperatures. Samples deposited at room temperature show hardness values lower than 5 GPa and improve slightly to a value of 7.9±0.5 GPa when deposited at the lowest pressure of 0.3 Pa. XRD patterns showed that thin films deposited at room temperature and high pressure are quasi-crystalline in nature, with coexistence of multiple Ti-Au intermetallics. Quasi-crystalline

nature behaves like a large number of defects uniformly distributed in the film, while the open void structure results in a lack of clear grain boundaries and together they weaken the material system [11,34]. These conditions improve with denser and better crystallized thin films, when the deposition pressure is lowered to 0.3 Pa, which is reflected in an improvement of hardness. With increase in substrate temperature to 275 and 350℃, the hardness values rise from 7 to 10 GPa when the deposition pressure is reduced from 1.2 to 0.3 Pa. This increase in hardness can be explained by the emergence of super-hard β-phases of Ti₃Au, which exist in denser atomic coordination and lead to formation of shorter atomic bonds resulting in higher hardness [26,27]. The presence of the α-phase, evidenced by the SEM and XRD results, also aids the improvement in hardness as it acts like a secondary phase defect particle in the β-Ti₃Au matrix, increasing the resistance to dislocation movement in the thin film. When the substrate temperature reaches

450°C, the hardness value jumps to 10 ± 0.7 GPa for films grown at a deposition pressure of 1.2 Pa, and continues to increase with further reduction in deposition pressure, reaching a peak hardness value of 12.5 ±1 GPa at a deposition pressure of 0.3 Pa. Material systems can be hardened by increasing the dislocation energy barrier through increasing the density of point/line defects, precipitation of super hard intermetallic phases, densification of columnar structures, increasing the grain boundaries by size reduction, or increasing the solute/secondary phase density within an alloy matrix [11,57,58]. It can be seen in Fig. 7(e) that increasing the substrate temperature leads to higher hardness in these intermetallic thin films, as the increase in adatom mobility and inter-grain diffusion leads to better crystallization of the super-hard β-Ti$_3$Au phase, as seen from the XRD patterns and calculated crystallite sizes in Fig. 3. Similarly, the improvement in hardness value with decrease in deposition pressure is also very evident in Fig. 7(e), as the decreasing deposition pressure causes densification of the films and flattening of the surface, as proven from the SEM images and AFM feature size measurements in previous sections. It is known that smaller grain sizes report larger internal grain boundaries, which increase the resistance to dislocation propagation, making the resulting thin films harder [59]. Therefore, by optimising substrate temperature, better crystallization of super-hard β-Ti$_3$Au can be achieved, whereas deposition pressure can be used to control the grain size by regulating the grain boundary diffusion and the packing density of the columnar features of these thin films.

Reduced modulus values measured for Ti$_3$Au thin films deposited on Ti$_6$Al$_4$V substrates with varying substrate temperature and deposition pressure are presented in Fig. 7(d). Samples deposited at room temperature report the lowest modulus values, starting from 65 ± 4 GPa for a deposition pressure of 1.2 Pa and then steadily increasing to 101 ± 11 GPa when the deposition pressure is reduced to 0.3 Pa. It can be seen from Fig. 7(d) that most of the thin films deposited on Ti-based substrates report slightly higher elastic modulus values, when compared their glass counterparts in Fig. 7(c), which can be related to the higher elastic modulus of the underlying Ti$_6$Al$_4$V substrate (114GPa) compared to the glass substrate (73GPa) [60,61]. During nanoindentation, substrate effects on hardness measurement can be minimised by limiting the indentation depth to 10% of the film thickness, but because of its larger field of interaction, elastic modulus is more easily affected by the stiffness of the underlying substrate, even at these limited indentation depths [61]. In earlier works, Ti$_3$Au intermetallic thin films were reported to have higher elastic modulus of around 200 GPa [11,27] which can be linked to the higher elastic modulus of the Si substrates (172GPa) used in those studies [61]. The lower elastic modulus of Ti$_3$Au thin films coated over Ti$_6$Al$_4$V substrates is favourable for the development of knee and hip implants, to aid the reduction of the stress shielding effect, which can cause poor bone re-growth and lead to costly reconstruction surgery [62].

The hardness results of the thin films deposited on Ti$_6$Al$_4$V substrates are shown in Fig. 7(f) and follow a similar pattern to the ones seen for glass substrates (Fig 7e). For films grown at room temperature, the hardness increases from 4.6 to 6.4 GPa with reduction in deposition pressure from 1.2 to 0.3 Pa, and this trend shows step increases in values from 7.8 to 9.5, 8.1 to 9.8 and 10.8 to 11.7 GPa, when the substrate temperature is subsequently increased to 275, 350 and 450°C, respectively. For films deposited on Ti$_6$Al$_4$V substrates, a peak hardness value of 11.7 ± 1.3 GPa is achieved when the deposition pressure is reduced to 0.3 Pa and the substrate temperature is set to 450°C. One significant difference in the results for thin films deposited on Ti-based substrates, is the larger error bars on the data points when compared to their glass counterparts. On Ti$_6$Al$_4$V substrates, the size of the error bars increases between 2 to 8 times for elastic modulus results and 2 to 4 times for hardness results when compared to the results on glass substrates. Previous works have demonstrated that an increase in surface roughness leads to widening of the scatter for data measured using the nanoindentation method [55,63-65]. Even though the Ti$_6$Al$_4$V substrates

underwent a rigorous polishing process to achieve a surface finish better than 40 nm, they are still much rougher when compared to glass substrates with roughness values lower than 2 nm. Despite the larger error bars, the mean values for elastic modulus and hardness on both substrate types are in very good agreement with each other.

The peak hardness values of 12.5 and 11.7 GPa achieved for Ti$_3$Au thin films deposited at a substrate temperature of 450°C and deposition pressure of 0.3 Pa on glass and Ti$_6$Al$_4$V alloy substrates, respectively, are in good agreement with our previous work on thermal activation of Ti$_{(1-x)}$Au$_{(x)}$ films with in-situ (11.9 GPa) and ex-situ (12.3 GPa) heat treatment [31] as well as the results of Karimi *et al.* on crystalline β-Ti$_3$Au thin films (10.4 to 12.1 GPa) [27]. These hardness values are ~1.5 times higher than that achieved by Svanidze *et al.* for bulk β-Ti$_3$Au alloys prepared by arc melting (~7.85 GPa) [26] and over 3 times higher than the hardness of Ti$_6$Al$_4$V (3.9 GPa) [66] and CoCr (3.7 GPa) [67] alloy ball heads currently used in most metal hip implants. Moreover, the hardness values of the Ti$_3$Au thin films achieved in this work are also comparable to that of state-of-the-art implant materials such as oxidised zirconium (Oxinium), which is known to have a surface hardness value over 2 times higher than CoCr but can be susceptible to accelerated wear if the oxidised surface gets damaged and reveals the relatively soft underlying zirconium alloy [68].

3.4. Biocompatibility results

The biocompatibility of the Ti$_3$Au thin films deposited on Ti$_6$Al$_4$V substrates was analysed by preparing their extracts (as described in materials and methods 2.4), to test the leaching potential and the cytotoxicity of these leached elements on the host cells, see Fig. 8(a). It is worth mentioning that all obtained extracts were used undiluted, in order to explore the maximum rate of any potential cytotoxic effect of the Ti$_3$Au thin films against L929 mouse fibroblasts. Data analysis revealed that almost all tested extracts made from these thin films showed excellent biocompatibility, possessing a safe cytotoxic profile against L929 mouse fibroblasts over an incubation period of 72 hours, see Fig. 8(b). Viability levels were slightly affected, appearing between 80 to 90% when compared to untreated (Blank) samples (green and blue dashed lines in Fig. 8(b)). Such response was not only observed following exposures with extracts obtained from 72 hours of ion leaching, but also after incubations with extracts obtained from prolonged 168 hour ion leaching periods. Only two samples, S$_{275-9}$ and S$_{450-12}$ caused a decrease of cell viability values between 70 and 80% after exposures with extracts from 168 hours of ion leaching, but according to ISO 10993 standards are still considered as biocompatible [69,70]. On the other hand, although sample S$_{RT-12}$ did not cause a significant decrease of L929 cell viability levels (above 85% when compared to Blank samples) after exposures with extracts obtained from 72 hours of ion leaching, incubations with extracts derived from 168 hours of leaching, induced a 30% reduction of cell viability levels. Lower substrate temperature and higher deposition pressure, as in the case of sample S$_{RT-12}$, leads to the formation of a broken columnar structure with larger voids (zone 1 texture), which in turn increases the surface area available for ion leaching, ultimately resulting in decreased rates of cell viability [34,71,72]. In addition, blank Ti substrates also recorded strong biocompatibility and were shown to further stimulate L929 cell viability levels, a response also observed in exposures with S$_{275-12}$, S$_{350-12}$, S$_{450-6}$ and S$_{450-12}$ extracts obtained following 72 hours of ion leaching (Fig. 8(b)). In contrast, both exposures with Cu substrates and 10% DMSO derived extracts had a strong cytotoxic effect, resulting in a dramatic increase of cell death rates. The toxicity of Cu ions in mammalian cells originates from oxidative damage and breakage of DNA bonds which leads to cell apoptosis [14]. In summary, it can be observed that Ti$_3$Au thin films deposited at higher substrate temperature and lower pressure tend to exhibit a safer cytotoxic profile when compared to those deposited at lower substrate temperature and higher pressure.
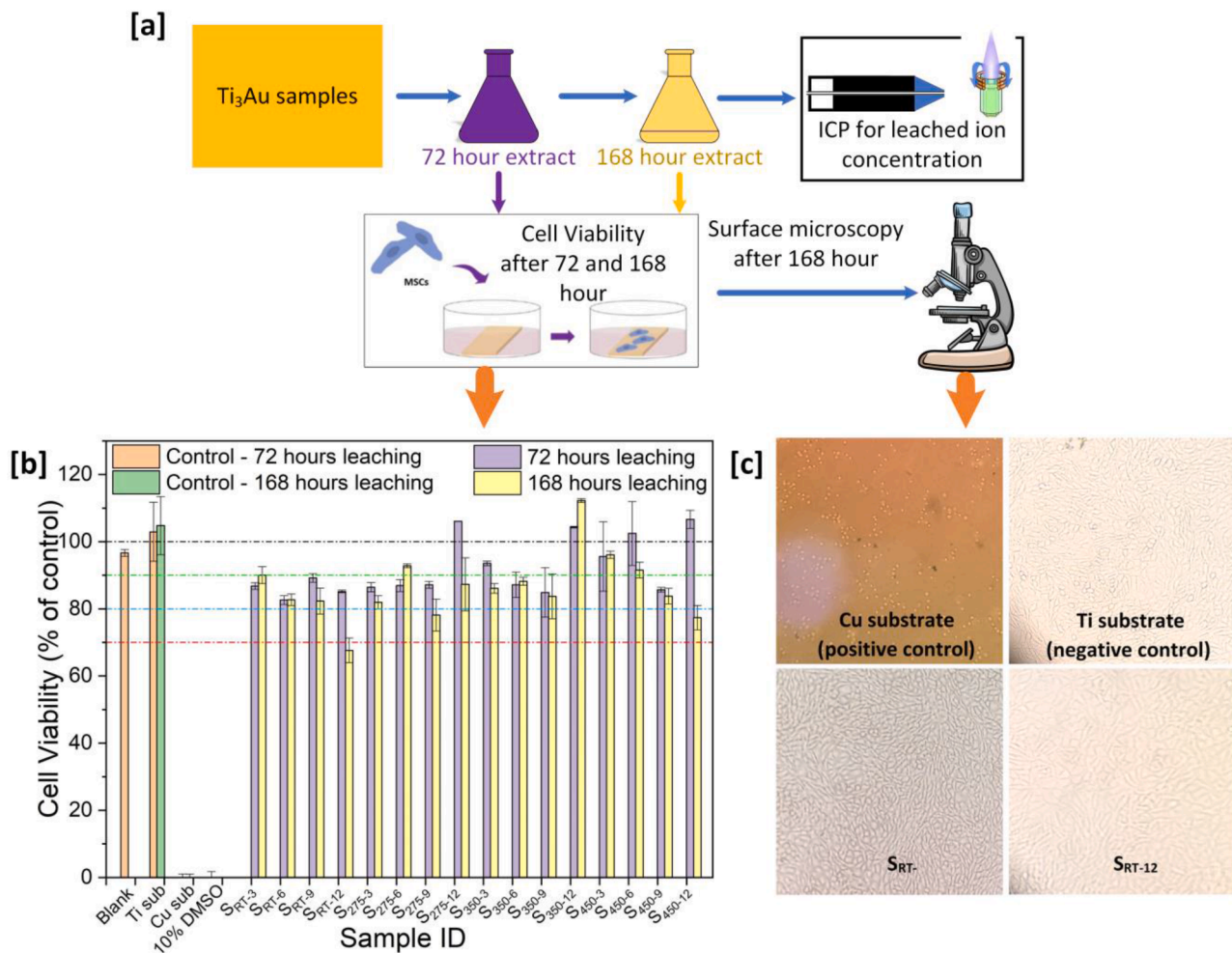
Fig. 8. (a) Schematic of the biocompatibility characterization process flow (b) Cytotoxic effect of extracts leached from Ti_3Au thin films deposited on Ti substrates at varying substrate temperatures and deposition pressures, against L929 mouse fibroblast cells, following 72 hours of exposure, compared to negative (untreated (BLANK) and Ti substrate) and positive controls (Cu substrate and 10% DMSO). (c) Morphological changes of L929 mouse fibroblast cells following 72 hours of incubation with a Cu substrate (positive control), Ti substrate (negative control), SRT-3 and SRT-12 Ti_3Au thin film extracts, obtained after 168 hours of ion leaching. Images were acquired using an inverted Kern microscope with attached digital camera and 10X lens.

Moreover, we have observed differences in L929 cell morphology following exposure with material extracts, see Fig. 8(c). Specifically, incubations with Cu substrate extracts obtained from 168 hours of ion leached media caused cell shrinkage and death of L929 mouse fibroblasts, resulting in confluency reduction. In contrast, the cell shape and morphology of L929 cells following incubations with Ti substrate extracts and S_{RT-3} extracts were not altered, confirming their safe cytotoxic and biocompatible nature. Interestingly this pattern of cell shape and morphology as well as density of L929 cells, was also observed in incubations with S_{RT-12} samples, although associated with the lowest cell viability rates (approximately 70%), when compared to those of the other tested Ti_3Au thin films.

Next, the ICP-OEMS assay was employed in order to measure the average level of ions leached from each of these samples, when immersed in DMEM for 72 and 168 hours for extract preparation purposes. Four calibration solutions, with known ion concentrations of 0.625, 2.5, 5 and 10 ppm for Ti, Au and Cu, were prepared. In the case of extracts obtained from Cu substrates (positive control), an ion concentration in excess of 89 ppm was observed with 72 hours of leaching, which increased to 112 ppm after 168 hours of leaching. Earlier studies have shown that Cu ion concentrations in excess of 10 ppm display cytotoxic behaviour towards the host cells [23,24,73]. Such behaviour is in accordance with the observed extremely high cytotoxic potential of Cu derived extracts against L929 cells. On the other hand, the blank Ti substrate (negative control) and Ti_3Au thin films did not show any significant ion leaching properties, a condition accompanied by a safe cytotoxic profile against mouse fibroblast cells. After 72 hours of leaching, the highest Ti concentration detected in the Ti_3Au thin film extracts did not exceed 0.4 ppm and was observed in the extract derived from the S_{450-9} sample, whereas the Au concentration was below the detection limit of the system, existing in the ppb range. Even after leaving the test samples in the extract medium for further 96 hours (total 168 hours), the Ti concentration only increased by a further 0.13 - 0.14 ppm across all samples, with Au ion concentrations still registering in the ppb range. The difference in the ion concentrations after 72 and 168 hours also shows that the ion release rate for Ti-Au ions from Ti_3Au intermetallic alloy thin films steadily decrease in biological fluids. Overall, the combined ion concentration in any of the Ti_3Au thin film extracts, irrespective of leaching duration, was found to be below 0.54 ppm, a value that is extremely low when compared to the toxicity threshold of 10 ppm explained above.

4. Conclusion

This work presents a new method to enhance the mechanical performance of the super-hard biocompatible β-Ti_3Au intermetallic in thin film form by controlling its microstructure development using gas pressure and substrate temperature deposition parameters. This study

clearly demonstrates that the Ti$_3$Au intermetallic deposited at higher gas pressures and without any substrate temperature forms a quasi-crystalline structure, as predicted for thin films in zone 1 of Thorntons SZM due to a reduction of adatom mobility in this zone. This quasi-crystalline structure can be developed into a preferentially oriented β-phase by increasing the adatom mobility, achieved by increasing the substrate temperature and lowering the deposition gas pressure. Grain size and surface roughness can be predicted by following the SZM to achieve better β-phase crystallization with smaller grain size, to increase the hardness of this intermetallic system. There is a steady increase in hardness and elastic modulus with increasing substrate temperature to 450°C and decreasing gas pressure to 0.3 Pa, with peak values of 12.4 GPa and 150 GPa achieved, respectively. In parallel, all tested Ti$_3$Au thin films are found to be highly biocompatible with minimally affected L929 cell viability levels, in exposures with extracts obtained from both short (72 hour) and long (168 hour) periods of ion leaching, especially regarding films deposited at lower gas pressure and higher substrate temperature. On the other hand, the observed slight reduction of cell viability levels for some deposition parameter combinations following prolonged exposure of 168 hours, is correlated to an increase of ions leaching into the extracts due to increased film surface area related to changes in film microstructure and texture. This work has shown that microstructure modification, by fine tuning sputter deposition parameters, can be efficiently utilised to develop highly biocompatible Ti$_3$Au thin films with high hardness (>12GPa) and low elastic modulus (<150GPa) with future potential as a coating material system to prolong the lifetime of Ti-based artificial joint implants.

CRediT authorship contribution statement

Cecil Cherian Lukose: Investigation, Formal analysis, Validation, Data curation, Visualization, Writing – original draft. **Ioannis Anestopoulos:** Investigation, Formal analysis, Validation, Writing – review & editing. **Leon Bowen:** Methodology, Investigation, Formal analysis. **Mihalis I. Panayiotidis:** Investigation, Conceptualization, Methodology, Writing – review & editing, Supervision, Funding acquisition. **Martin Birkett:** Investigation, Conceptualization, Methodology, Writing – review & editing, Supervision, Project administration, Funding acquisition.

Declaration of Competing Interest

The authors declare that they have no known competing financial interests or personal relationships that could have appeared to influence the work reported in this paper.

Data availability

Data will be made available on request.

Acknowledgement

Supplementary materials

Supplementary material associated with this article can be found, in the online version, at doi:10.1016/j.surfin.2023.103034.

References

[1] M. Abdel-Hady Gepreel, M. Niinomi, Biocompatibility of Ti-alloys for long-term implantation, J Mech Behav Biomed 20 (2013) 407–415.

[2] A. Nemati, M. Saghafi, S. Khamseh, E. Alibakhshi, P. Zarrintaj, M.R. Saeb, Magnetron-sputtered TixNy thin films applied on titanium-based alloys for biomedical applications: Composition-microstructure-property relationships, Surf Coat Tech 349 (2018) 251–259.

[3] C.M. Han, H.E. Kim, Y.S. Kim, S.K. Han, Enhanced biocompatibility of Co-Cr implant material by Ti coating and micro-arc oxidation, J Biomed Mater Res B 90 (2009) 165–170.

[4] A.P.I. Popoola, L. Phume, S. Pityana, V.S. Aigbodion, In-situ formation of laser Ti6Al4V–TiB composite coatings on Ti6Al4V alloy for biomedical application, Surf Coat Tech 285 (2016) 161–170.

[5] Y. Zhao, J. Xu, S. Peng, Synthesis and evaluation of TaC nanocrystalline coating with excellent wear resistance, corrosion resistance, and biocompatibility, Ceram Int 47 (2021) 20032–20044.

[6] R.A. Roşu, V.A. Şerban, A.I. Bucur, U. Dragoş, Deposition of titanium nitride and hydroxyapatite-based biocompatible composite by reactive plasma spraying, Appl Surf Sci 258 (2012) 3871–3876.

[7] S. Ozan, J. Lin, Y. Li, R. Ipek, C. Wen, Development of Ti-Nb-Zr alloys with high elastic admissible strain for temporary orthopedic devices, Acta Biomater 20 (2015) 176–187.

[8] D.L. Alontseva, E. Ghassemieh, S. Voinarovych, A. Russakova, O. Kyslytsia, Y. Polovetskyi, A. Toxanbayeva, Characterisation of the microplasma spraying of biocompatible coating of titanium, J Microsc 279 (2020) 148–157.

[9] W. Cui, G. Qin, J. Duan, H. Wang, A graded nano-TiN coating on biomedical Ti alloy: Low friction coefficient, good bonding and biocompatibility, Mater Sci Eng C-Mater 71 (2017) 520–528.

[10] M. Rajagopalan, R.Rajiv Gandhi, First principles study of structural, electronic, mechanical and thermal properties of A15 intermetallic compounds Ti3X (X=Au, Pt, Ir), Physica B 407 (2012) 4731–4734.

[11] C. Lopes, C. Gabor, D. Cristea, R. Costa, R.P. Domingues, M.S. Rodrigues, J. Borges, E. Alves, N.P. Barradas, D. Munteanu, F. Vaz, Evolution of the mechanical properties of Ti-based intermetallic thin films doped with different metals to be used as biomedical devices, Appl Surf Sci 505 (2020), 144617.

[12] E. Unosson, D. Rodriguez, K. Welch, H. Engqvist, Reactive combinatorial synthesis and characterization of a gradient Ag-Ti oxide thin film with antibacterial properties, Acta Biomater 11 (2015) 503–510.

[13] D. Wojcieszak, M. Mazur, D. Kaczmarek, P. Mazur, B. Szponar, J. Domaradzki, L. Kepinski, Influence of the surface properties on bactericidal and fungicidal activity of magnetron sputtered Ti-Ag and Nb-Ag thin films, Mater Sci Eng C-Mater 62 (2016) 86–95.

[14] D. Wojcieszak, D. Kaczmarek, A. Antosiak, M. Mazur, Z. Rybak, A. Rusak, M. Osekowska, A. Poniedzialek, A. Gamian, B. Szponar, Influence of Cu-Ti thin film surface properties on antimicrobial activity and viability of living cells, Mater Sci Eng C-Mater 56 (2015) 48–56.

[15] D. Wojcieszak, M. Mazur, M. Kalisz, M. Grobelny, Influence of Cu, Au and Ag on structural and surface properties of bioactive coatings based on titanium, Mater Sci Eng C-Mater 71 (2017) 1115–1121.

[16] V. Stranak, H. Wulff, H. Rebl, C. Zietz, K. Arndt, R. Bogdanowicz, B. Nebe, R. Bader, A. Podbielski, Z. Hubicka, R. Hippler, Deposition of thin titanium–copper films with antimicrobial effect by advanced magnetron sputtering methods, Mater Sci Eng C-Mater 31 (2011) 1512–1519.

[17] G.A. Norambuena, R. Patel, M. Karau, C.C. Wyles, P.J. Jannetto, K.E. Bennet, A. D. Hanssen, R.J. Sierra, Antibacterial and Biocompatible Titanium-Copper Oxide Coating May Be a Potential Strategy to Reduce Periprosthetic Infection: An In Vitro Study, Clin Orthop Relat Res 475 (2017) 722–732.

[18] M. Takahashi, Y. Kikuchi M Fau - Takada, O. Takada Y Fau - Okuno, O. Okuno, Mechanical properties and microstructures of dental cast Ti-Ag and Ti-Cu alloys, Dent Mater J 21 (2002) 270–280.

[19] M. Kikuchi, Y. Takada, S. Kiyosue, M. Yoda, M. Woldu, Z. Cai, O. Okuno, T. Okabe, Mechanical properties and microstructures of cast Ti–Cu alloys, Dent Mater 19 (2003) 174–181.

[20] M. Kikuchi, Y. Takada, S. Kiyosue, M. Yoda, M. Woldu, Z. Cai, O. Okuno, T. Okabe, Grindability of cast Ti–Cu alloys, Dent Mater 19 (2003) 375–381.

[21] M. Takahashi, M. Kikuchi, Y. Takada, O. Okuno, Grindability and mechanical properties of experimental Ti–Au, Ti–Ag and Ti–Cu alloys, Int Congr Ser 1284 (2005) 326–327.

[22] A. Shi, C. Zhu, S. Fu, R. Wang, G. Qin, D. Chen, E. Zhang, What controls the antibacterial activity of Ti-Ag alloy, Ag ion or Ti2Ag particles? Mater Sci Eng C-Mater 109 (2020), 110548.

[23] W.M. Elshahawy, I. Watanabe, P. Kramer, In vitro cytotoxicity evaluation of elemental ions released from different prosthodontic materials, Dent Mater 25 (2009) 1551–1555.

[24] A. Milheiro, K. Nozaki, C.J. Kleverlaan, J. Muris, H. Miura, A.J. Feilzer, In vitro cytotoxicity of metallic ions released from dental alloys, Odontology 104 (2016) 136–142.

[25] R.J. Kadhim, E.H. Karsh, Z.J. Taqi, M.S. Jabir, Biocompatibility of gold nanoparticles: In-vitro and In-vivo study, Mater Today-Proc 42 (2021) 3041–3045.

[26] E. Svanidze, T. Besara, M.F. Ozaydin, C.S. Tiwary, J.K. Wang, S. Radhakrishnan, S. Mani, Y. Xin, K. Han, H. Liang, T. Siegrist, P.M. Ajayan, E. Morosan, High hardness in the biocompatible intermetallic compound β-Ti3Au, Sci Adv 2 (2016), e1600319.

[27] A. Karimi, C. Cattin, Intermetallic β-Ti3Au hard thin films prepared by magnetron sputtering, Thin Solid Films 646 (2018) 1–11.

[28] Y.-R. Lee, M.-K. Han, M.-K. Kim, W.-J. Moon, H.-J. Song, Y.-J. Park, Effect of gold addition on the microstructure, mechanical properties and corrosion behavior of Ti alloys, Gold Bull 47 (2014) 153–160.

[29] K.T. Oh, D.K. Kang, G.S. Choi, K.N. Kim, Cytocompatibility and electrochemical properties of Ti-Au alloys for biomedical applications, J Biomed Mater Res B 83 (2007) 320–326.

[30] O.N. Senkov, D.B. Miracle, Generalization of intrinsic ductile-to-brittle criteria by Pugh and Pettifor for materials with a cubic crystal structure, Sci Rep 11 (2021) 4531.

[31] C.C. Lukose, I. Anestopoulos, T. Mantso, L. Bowen, M.I. Panayiotidis, M. Birkett, Thermal activation of Ti(1-x)Au(x) thin films with enhanced hardness and biocompatibility, Bioact Mater 15 (2022) 426–445.

[32] B.A. Nejand, S. Sanjabi, V. Ahmadi, The effect of sputtering gas pressure on structure and photocatalytic properties of nanostructured titanium oxide self-cleaning thin film, Vacuum 85 (2010) 400–405.

[33] D. Song, A.G. Aberle, J. Xia, Optimisation of ZnO:Al films by change of sputter gas pressure for solar cell application, Appl Surf Sci 195 (2002) 291–296.

[34] E. Kusano, Structure-Zone Modeling of Sputter-Deposited Thin Films: A Brief Review, Appl Sci Converg Technol 28 (2019) 179–185.

[35] J.A. Thornton, Structure-Zone Models of Thin Films, Proceedings of SPIE 821 (1988) 95–103.

[36] T. Oya, E. Kusano, Effects of radio-frequency plasma on structure and properties in Ti film deposition by dc and pulsed dc magnetron sputtering, Thin Solid Films 517 (2009) 5837–5843.

[37] M.E.A.M.T. Hosseinnejad, N. Panahi, M.A. Ferdosi Zadeh, S.W. Case, Structural, morphological and mechanical hardness properties of titanium nitride thin films deposited by DC magnetron sputtering: Effect of substrate temperature, J Optoelectron Adv M 19 (2017) 434–439.

[38] P. Patsalas, C. Charitidis, S. Logothetidis, The effect of substrate temperature and biasing on the mechanical properties and structure of sputtered titanium nitride thin films, Surf Coat Tech 125 (2000) 335–340.

[39] S.Kumari Soni, S.K. Sharma, S.K. Mishra, Effect of Deposition Pressure, Nitrogen Content and Substrate Temperature on Optical and Mechanical Behavior of Nanocomposite Al-Si-N Hard Coatings for Solar Thermal Applications, J Mater Eng Perform 27 (2018) 6729–6736.

[40] S. Wu, H. Chen, X. Du, Z. Liu, Effect of deposition power and pressure on rate deposition and resistivity of titanium thin films grown by DC magnetron sputtering, Spectrosc Lett 49 (2016) 514–519.

[41] H.N. Shah, R. Jayaganthan, D. Kaur, Effect of sputtering pressure and temperature on DC magnetron sputtered CrN films, Surf Eng 26 (2013) 629–637.

[42] K.Y. Chan, B.S. Teo, Sputtering power and deposition pressure effects on the electrical and structural properties of copper thin films, J Mater Sci 40 (2005) 5971–5981.

[43] X. Wei, Y. Dong, D. Qu, T. Ma, J. Shen, Effect of Deposition Parameters on Microstructure of the Ti-Mg Immiscible Alloy Thin Film Deposited by Multi-Arc Ion Plating, Metals 9 (2019) 1229.

[44] E. Arslan, F. Bülbül, A. Alsaran, A. Celik, I. Efeoglu, The effect of deposition parameters and Ti content on structural and wear properties of MoS2Ti coatings, Wear 259 (2005) 814–819.

[45] J.H. Kim, S. Lee, H.S. Im, The effect of target density and its morphology on TiO2 thin films grown on Si(100) by PLD, Appl Surf Sci 151 (1999) 6–16.

[46] J. Sharma, S.K. Tripathi, Effect of deposition pressure on structural, optical and electrical properties of zinc selenide thin films, Physica B 406 (2011) 1757–1762.

[47] A.L. Patterson, The Scherrer Formula for X-Ray Particle Size Determination, Phys Rev 56 (1939) 978–982.

[48] J.L. Murray, The Au-Ti (Gold-Titanium) system, Bull Alloy Phase Diagr 4 (1983) 278–283.

[49] W.W. Gerberich, W.M. Mook, M.D. Chambers, M.J. Cordill, C.R. Perrey, C. B. Carter, R.E. Miller, W.A. Curtin, R. Mukherjee, S.L. Girshick, An Energy Balance Criterion for Nanoindentation-Induced Single and Multiple Dislocation Events, J Appl Mech 73 (2006) 327–334.

[50] Y. Wang, P.L. Tam, Y.G. Shen, Behavior of Ti0.5Al0.5N thin film in nanoscale deformation with different loading rates, Thin Solid Films 516 (2008) 7641–7647.

[51] S.G. Corcoran, R.J. Colton, E.T. Lilleodden, W.W. Gerberich, Nanoindentation Studies of Yield Point Phenomena on Gold Single Crystals, Mater Res Soc Symp Proc 436 (1996) 159–164.

[52] J. Ding, Y. Meng, S. Wen, Mechanical properties and fracture toughness of multilayer hard coatings using nanoindentation, Thin Solid Films 371 (2000) 178–182.

[53] C.T. Chuang, C.K. Chao, R.C. Chang, K.Y. Chu, Effects of internal stresses on the mechanical properties of deposition thin films, J Mater Process Tech 201 (2008) 770–774.

[54] A.K. Nanda Kumar, C.K. Sasidharan Nair, M.D. Kannan, S. Jayakumar, TEM and nanoindentation studies on sputtered Ti40Ni60 thin films, Mater Chem Phys 97 (2006) 308–314.

[55] W.G. Jiang, J.J. Su, X.Q. Feng, Effect of surface roughness on nanoindentation test of thin films, Eng Fract Mech 75 (2008) 4965–4972.

[56] Y. Xia, M. Bigerelle, J. Marteau, P.E. Mazeran, S. Bouvier, A. Iost, Effect of surface roughness in the determination of the mechanical properties of material using nanoindentation test, Scanning 36 (2014) 134–149.

[57] L. Hultman, Thermal stability of nitride thin films, Vacuum 57 (2000) 1–30.

[58] P.H. Mayrhofer, C. Mitterer, L. Hultman, H. Clemens, Microstructural design of hard coatings, Prog Mater Sci 51 (2006) 1032–1114.

[59] B.B. Jung, H.K. Lee, H.C. Park, Effect of grain size on the indentation hardness for polycrystalline materials by the modified strain gradient theory, Int J Solids Struct 50 (2013) 2719–2724.

[60] I. Sen, U. Ramamurty, Elastic modulus of Ti–6Al–4V–xB alloys with B up to 0.55wt. %, Scripta Mater 62 (2010) 37–40.

[61] R. Saha, W.D. Nix, Effects of the substrate on the determination of thin film mechanical properties by nanoindentation, Acta Mater 50 (2002) 23–38.

[62] M. Niinomi, M. Nakai, Titanium-Based Biomaterials for Preventing Stress Shielding between Implant Devices and Bone, Int J Biomater 2011 (2011), 836587.

[63] L. Chen, A. Ahadi, J. Zhou, J.-E. Ståhl, Modeling Effect of Surface Roughness on Nanoindentation Tests, Procedia CIRP 8 (2013) 334–339.

[64] N.G. Demas, C. Lorenzo-Martin, O.O. Ajayi, R.A. Erck, I. Shareef, Measurement of Thin-film Coating Hardness in the Presence of Contamination and Roughness: Implications for Tribology, Metall Mater Trans A 47 (2016) 1629–1640.

[65] C. Walter, T. Antretter, R. Daniel, C. Mitterer, Finite element simulation of the effect of surface roughness on nanoindentation of thin films with spherical indenters, Surf Coat Tech 202 (2007) 1103–1107.

[66] S. Skvortsova, A. Orlov, G. Valyano, V. Spektor, N. Mamontova, Wear Resistance of Ti-6Al-4V Alloy Ball Heads for Use in Implants, J Funct Biomater 12 (2021) 65.

[67] C.T. Duong, J.S. Nam, E.M. Seo, B.P. Patro, J.D. Chang, S. Park, S.S. Lee, Tribological property of the cobalt-chromium femoral head with different regions of wear in total hip arthroplasty, Proc Inst Mech Eng H 224 (2010) 541–549.

[68] L. Kore, T. Bates, G. Mills, D. Lybeck, Oxidized Zirconium Total Knee Arthroplasty Implant Failure in a Patient with Knee Instability, Arthroplast Today 6 (2020) 552–555.

[69] S. Frykstrand, J. Forsgren, P. Zhang, M. Strømme, N. Ferraz, Cytotoxicity, in Vivo Skin Irritation and Acute Systemic Toxicity of the Mesoporous Magnesium Carbonate Upsalite, J Biomate Nanobiotechnol 6 (2015) 257–266.

[70] ISO 10993-5 Biological evaluation of medical devices - part 5 - tests for in vitro cytotoxicity, 2009, pp. 34.

[71] M. Assad, A. Chernyshov, M.A. Leroux, C.H. Rivard, A new porous titanium–nickel alloy: Part 2. Sensitization, irritation and acute systemic toxicity evaluation, BioMed Mater Eng 12 (2002) 339–346.

[72] J.P.Y. Ho, S.L. Wu, R.W.Y. Poon, C.Y. Chung, S.C. Tjong, P.K. Chu, K.W.K. Yeung, W.W. Lu, K.M.C. Cheung, K.D.K. Luk, Oxygen plasma treatment to restrain nickel out-diffusion from porous nickel titanium orthopedic materials, Surf Coat Tech 201 (2007) 4893–4896.

[73] H. Libalova, P.M. Costa, M. Olsson, L. Farcal, S. Ortelli, M. Blosi, J. Topinka, A. L. Costa, B. Fadeel, Toxicity of surface-modified copper oxide nanoparticles in a mouse macrophage cell line: Interplay of particles, surface coating and particle dissolution, Chemosphere 196 (2018) 482–493.